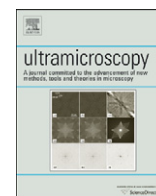




ELSEVIER

Contents lists available at [SciVerse ScienceDirect](http://www.sciencedirect.com)

Ultramicroscopy

journal homepage: www.elsevier.com/locate/ultramic

Imaging and strain analysis of nano-scale SiGe structures by tip-enhanced Raman spectroscopy

Peter Hermann^{a,b,c,*}, Michael Hecker^b, Dmytro Chumakov^b, Martin Weisheit^b, Jochen Rinderknecht^b, Artem Shelaev^d, Pavel Dorozhkin^d, Lukas M. Eng^e

^a Fraunhofer-Center Nanoelectronic Technologies, 01099 Dresden, Germany

^b Globalfoundries Dresden Module One LLC & Co. KG, 01109 Dresden, Germany

^c Robert Koch-Institute, 13353 Berlin, Germany

^d NT-MDT Co., 124482 Moscow, Russia

^e Institut für Angewandte Photophysik, Technische Universität Dresden, 01062 Dresden, Germany

ARTICLE INFO

Article history:

Received 20 April 2011

Received in revised form

22 July 2011

Accepted 5 August 2011

Available online 16 September 2011

Keywords:

Tip-enhanced Raman spectroscopy (TERS)

Enhanced Raman scattering

Spectroscopic imaging

Nano-scale chemical microscopy

Stress and strain in silicon

Silicon-germanium (SiGe)

ABSTRACT

The spatial resolution and high sensitivity of tip-enhanced Raman spectroscopy allows the characterization of surface features on a nano-scale. This technique is used to visualize silicon-based structures, which are similar in width to the transistor channels in present leading-edge CMOS devices. The reduction of the intensive far-field background signal is crucial for detecting the weak near-field contributions and requires beside a careful alignment of laser polarization and tip axis also the consideration of the crystalline sample orientation. Despite the chemical identity of the investigated sample surface, the structures can be visualized by the shift of the Raman peak positions due to the patterning induced change of the stress distribution within lines and substrate layer. From the measured peak positions the intrinsic stress within the lines is calculated and compared with results obtained by finite element modeling. The results demonstrate the capability of the tip-enhanced Raman technique for strain analysis on a sub-50 nm scale.

© 2011 Elsevier B.V. All rights reserved.

1. Introduction

The downscaling of semiconductor device dimensions, which was for decades the dominating technique for performance enhancement of leading edge complementary metal-oxide-semiconductor (CMOS) devices, is approaching more and more its physical and economic limits. Therefore, the implementation of new materials and techniques like strain engineering has become inevitable for the continuous performance improvement [1]. Tensile or compressive stress in the transistor channel generated e.g. by the lattice mismatch of silicon (Si) and silicon-germanium (Si:Ge) [2,3] or silicon-carbon (Si:C) [4,5] leads to a shift and splitting of the band structures, thus influencing the effective mass of charge carriers [6]. This selective introduction of strain in the active area of CMOS devices results in a further significant

* Corresponding author at: Biomedical Spectroscopy, Robert-Koch Institute, 13353 Berlin, Germany.

E-mail addresses: hermannp@rki.de (P. Hermann),

michael.hecker@globalfoundries.com (M. Hecker),

dmytro.chumakov@amd.com (D. Chumakov),

martin.weisheit@globalfoundries.com (M. Weisheit),

jochen.rinderknecht@globalfoundries.com (J. Rinderknecht),

artem.shelaev@ntmdt.ru (A. Shelaev), pavel.dorozhkin@ntmdt.ru (P. Dorozhkin),

lukas.eng@iapp.de (L.M. Eng).

performance improvement [7]. However, the optimization of the strain distribution requires also non-destructive and fast analytical methods with the capability of characterizing Si-based structures of comparable dimensions as transistors in present CMOS devices. Due to the sensitivity of lattice vibrations (phonons) to strain [8], Raman spectroscopy has been widely used for stress investigation in semiconductor device structures [9–12]. The resolution of this technique is however limited by diffraction, making strain analysis in features smaller than $\sim \lambda/2$ impossible. The discovery of surface-enhanced Raman scattering [13] not only significantly increased the sensitivity of this spectroscopic technique but provided with tip-enhanced Raman (TER) scattering [14,15] also a nm-scale light source with the capability of reaching a spatial resolution required for strain characterization of leading edge CMOS devices [16–20]. The achievement of a spatial resolution of about 10 nm has been already demonstrated on samples with diminishing low background signal like carbon nanotubes [21,22] or different monolayers [23,24]. For TER measurements on opaque samples like Si a backscattering or reflection setup is required, enabling only the use of long working distance objectives with relatively low numerical aperture. Thus, the intensive far-field background signal makes the achievement of a comparable high resolution still challenging. In the present work TER investigations are performed on SiGe line structures of comparable dimensions as encountered in present CMOS devices. For obtaining a high signal

enhancement and reducing the intensive far-field background signal simultaneously, the orientation of the crystalline sample is also taken into account for the alignment procedure. Additionally, for a better understanding of the observed peak shifts, the stress distribution within lines and substrate are calculated by finite element modeling.

2. Experimental

The measurements described in the present work were performed on a backscattering TER system equipped with an atomic force microscope (AFM) (NT-MDT, Russia), a Raman spectrometer (NTEGRA spectra (upright)) and a diode laser with 473 nm excitation wavelength (Fig. 1a). The laser beam was focused on the sample surface and tip-apex by a long working distance objective (Mitutoyo, $100\times$ magnification, NA=0.7). In order to avoid heat induced shifts of the phonon bands, the laser power on the sample was reduced below 1 mW. The integration time for the acquired Raman spectra was 5 s. For an accurate alignment of the incident laser polarization along the tip axis, the system was additionally equipped with a polarizer ($\lambda/2$ -wave plate) allowing an in plane rotation of the laser polarization. The investigated SiGe structures with a line width in the sub-50 nm range were prepared by local anodic oxidation [25,26] in combination with subsequent wet chemical etching. This patterning technique allows a defined modification of the strain distribution on nm-scale while keeping the lattice defect density low compared to other patterning methods, e.g. focused ion beam

milling. For patterning, a sample with a fully strained 50 nm thick $\text{Si}_{76.1}\text{Ge}_{23.9}$ layer epitaxially grown on (0 0 1) Si substrate was used. In Fig. 1b, a scanning electron microscope (SEM) image with detailed dimensions of the SiGe pattern is shown. The five lines, about $15\ \mu\text{m}$ long, oriented along the $\langle 1\ 0\ 0 \rangle$ crystal axis had a height of about 40 nm while the thickness of the fully strained SiGe layer was reduced to about 10 nm due to the anisotropic etching process (Fig. 2b). For the TER measurements non-contact ATEC Si-AFM cantilevers (NanoWorld AG, Switzerland) coated with a $\sim 35\ \text{nm}$ thick Ag layer were used (SEM image Fig. 2a). For the alignment of tip and laser, the polarization of the incident beam was set along the tip axis by the $\lambda/2$ -wave plate. After placing the tip on a plane and homogenous sample area the surface was scanned by the laser using piezoelectrically driven mirrors. The obtained intensity map (Fig. 2b with cross section c) allowed a reproducible and accurate determination of the best tip position within the laser focus for TER measurements. The stress distribution within the SiGe lines and SiGe/Si substrate was calculated using a finite element modeling software (ANSYS 9.0). For modeling a free surface on the top and periodic boundary conditions on the right and left side of the modeled volume were assumed.

3. Results and discussion

A challenge for nano-scale investigations on Si-based samples arises from **the near-field to far-field sample volume ratio**, which

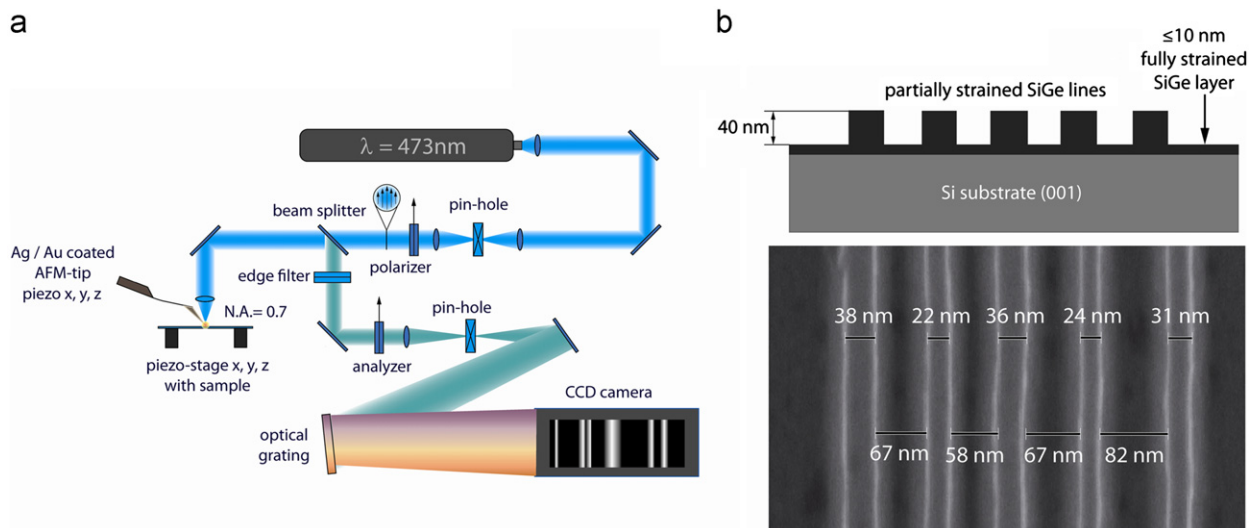


Fig. 1. (a) Experimental setup used for TER measurements on Si-based samples. (b) Schematic cross section and SEM image from the SiGe line structures obtained by local anodic oxidation and subsequent wet chemical etching. After etching a remnant $\leq 10\ \text{nm}$ thick fully strained SiGe layer was left on the (0 0 1) Si substrate. The SiGe lines have a height of about 40 nm and a length of $\sim 15\ \mu\text{m}$.

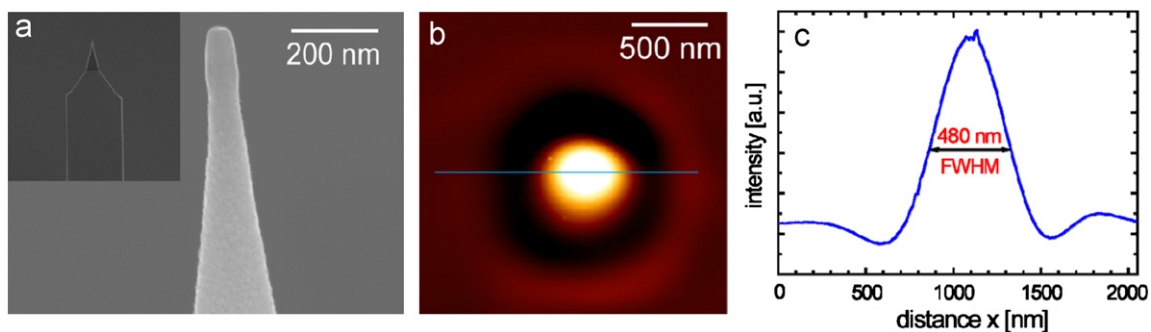


Fig. 2. (a) SEM image from ATEC-NC Si cantilever coated with a $\sim 35\ \text{nm}$ thick Ag film ($\varnothing \approx 50\ \text{nm}$). (b) Scattered intensity obtained from TER-tip by scanning the area around the tip apex with the laser focus. (c) Cross section of the measured intensity along the line marked in Fig. 2b.

makes the extraction of the small surface signal variations from the intensive background signal extremely difficult [27]. For high resolution measurements it is therefore inevitable to increase the near-field to far-field signal ratio. For this purpose different approaches applying polarization optics are increasingly used to obtain a high contrast by reducing the far-field contribution [19,20] of the acquired signal. A detailed overview about the different TER configurations as well as the used polarizer/analyzer settings can be found in Ref. [28]. The intensity of the backscattered Raman light depends on the crystal orientation of the sample as well as the polarization of the incident laser beam. Lee et al. [19] reported that by applying polarization optics for TER measurements on Si based samples, the contrast can be improved significantly by reducing the far-field contribution. The disadvantage of the approach described in Ref. [19] is that by rotating the polarization of the incident laser the electric field vector component along the tip axis decreases, thus also reducing the field enhancement at the tip apex [29,30]. Additionally, the scattering of laser light and depolarization at the tip and surface structures can induce the appearance of normally forbidden Raman modes. This makes the determination of the near-field contribution to the detected Raman signal difficult [31], since these far-field contributions cannot be completely suppressed by polarization optics. For the experiments described in the present article the polarization of the incident laser light is aligned in such a way that a strong electric field component along the tip axis [29,30] can be ensured. In order to significantly reduce the intensive far-field background signal the orientation of the crystalline sample is also taken into account for the alignment procedure. For this purpose the sample is mounted on a self-made rotation stage and fixed on the piezo-stage. After laser-tip-alignment, the appropriate orientation of the sample is determined by retracting the tip from the sample surface and rotating the sample stepwise while the laser polarization remains unchanged. According to the selection rules for backscattering from a (0 0 1) Si surface only the longitudinal optical phonon (LO) modes contribute to the far-field Raman signal [32,33] and the highest signal intensity is obtained, for a laser polarization along the (1 1 0) crystal axis (Fig. 3a). For a sample orientation with the (1 0 0) crystal axis parallel to the polarization of the incident laser light, the intensity of the backscattered Raman signal decreases by more than 99% compared to the configuration where the (1 1 0) crystal axis and the laser polarization are parallel. The same effect can be achieved, if instead of the sample the laser polarization is rotated around the (0 0 1) crystal axis and adjusted parallel to the (1 1 0) axis of the sample. However, this laser polarization would reduce the component of the electric field vector

along the axis of the TER tip, thus decreasing also the enhanced electromagnetic field at the apex. The configuration of incident laser polarization and crystalline sample orientation described in the present work prevents an efficient excitation of phonons due to the electromagnetic field distribution within the laser focus. Therefore, the signal intensity in far-field measurements is significantly reduced. When a metalized tip is moved into the laser spot a strong electromagnetic field can be generated under optimized conditions around the laser-irradiated TER tip. This enhanced electromagnetic field increases not only the intensity of the Raman signal but enables also a more efficient excitation of phonons in the close proximity of the tip apex due to the modulation of the electric field distribution [34]. For the following TER measurements on the SiGe structures the laser polarization is set along the tip axis while the intensive far-field background signal is reduced by rotating the crystalline sample to a (1 0 0) orientation parallel to the incident laser polarization.

In Fig. 3b two spectra acquired from the unpatterned area of the sample with a 50 nm thick fully strained SiGe layer on Si substrate are shown. For the reference spectrum (black) the laser is focused on the sample and the tip retracted by several μm from the surface. Due to the penetration depth of about 450 nm for the used excitation wavelength the Raman bands from layer and substrate appear in both spectra. Compared to the reference spectrum, the intensity of the Si-Si mode from layer and substrate is enhanced in the TER spectrum by 240% and 144%, respectively. Since Si substrate and tip apex are separated by the 50 nm thick SiGe layer, the observed enhancement of the substrate signal cannot be attributed to near-field contribution. This increase can be explained to one part by the tip material, since the Ag coating is only around the apex about 35 nm thick, thus not providing a complete suppression of the Si Raman signal from the whole laser-irradiated part of the TER tip. Another contribution to the increased Si signal intensity is the scattering of laser light by the metalized tip leading to minor polarization changes and therefore preventing a complete suppression of the Raman signature from the Si substrate. The influence of scattering on the measured Raman signal intensity is also visible in Fig. 4, showing the results obtained from a scan across the five SiGe lines with a retracted tip. The cross section data and the corresponding maps in Fig. 4 illustrate the intensity of both Si-Si modes in the interval from 519 cm^{-1} to 522 cm^{-1} and 507 cm^{-1} to 512 cm^{-1} showing an increase of the Raman signal for SiGe and Si substrate around of the patterns. While the increase of the Si-Si mode from SiGe can be explained by the higher average layer thickness and

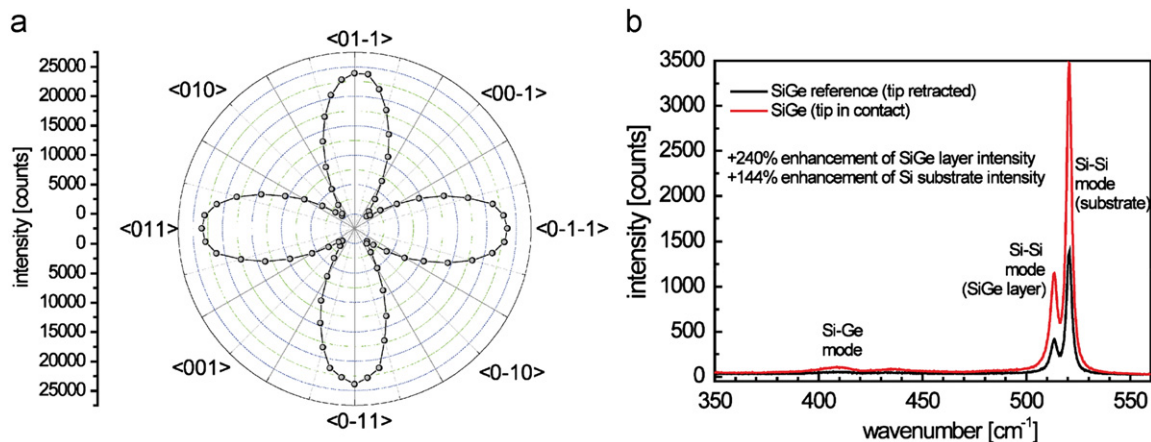


Fig. 3. (a) Intensity distribution of the backscattered Raman signal (Si-Si mode from Si substrate) from a (0 0 1) surface showing the strong dependence of the crystallographic sample orientation (for constant incident laser polarization \vec{E}). The highest Raman intensity is obtained if $\{1\ 1\ 0\} \parallel \vec{E}$, the lowest intensity for $\{1\ 0\ 0\} \parallel \vec{E}$. (b) Spectra showing the first order Raman modes from SiGe and Si substrate acquired from the sample before LAO patterning (50 nm thick SiGe layer). Compared to the reference spectrum (black) obtained with a retracted tip, all modes are enhanced by more than 100% when the tip is feedback (red). (For interpretation of the references to color in this figure legend, the reader is referred to the web version of this article.)

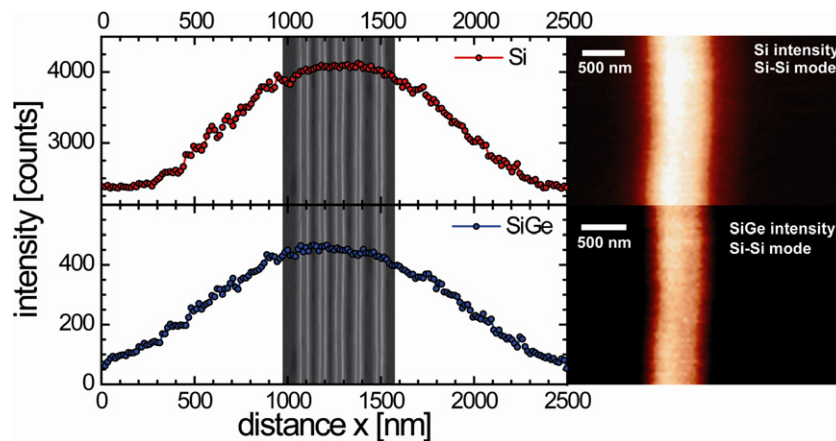


Fig. 4. Cross section data (left) and intensity map (right) of the Si–Si modes from layer and substrate obtained from a far-field Raman scan across the sample. In the images the intensity variations in the interval from 519 cm^{-1} to 522 cm^{-1} and 507 cm^{-1} to 512 cm^{-1} are shown.

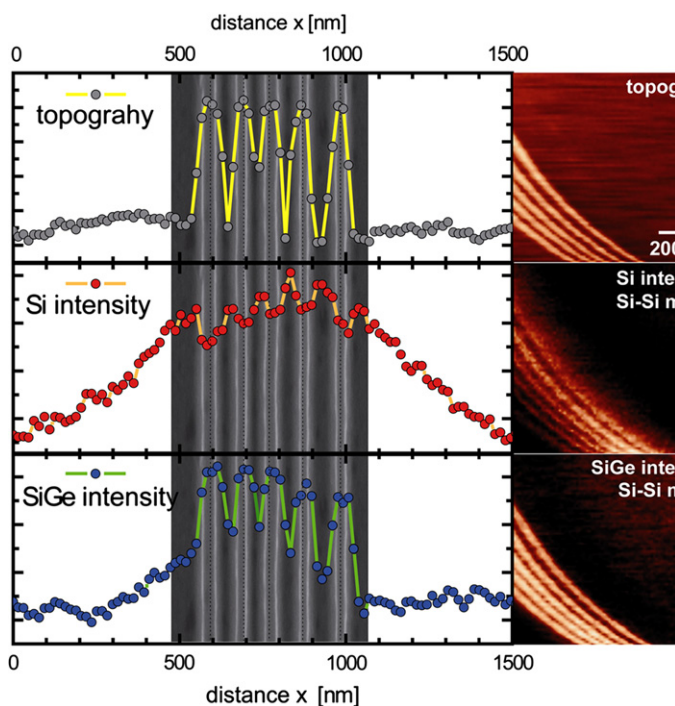


Fig. 5. Topography and Raman intensity cross section data (left) obtained from the first line scan of a $2\text{ }\mu\text{m} \times 2\text{ }\mu\text{m}$ large TER map of the five SiGe lines. On the right side an image section from the corresponding AFM/TER map is shown. For the Si–Si substrate the intensity variations in the interval between 519 cm^{-1} to 522 cm^{-1} are displayed in the line scan and intensity map while for the SiGe layer the changes between 507 cm^{-1} and 512 cm^{-1} are shown. The two intervals are also marked in the spectra presented in Fig. 6a. The slight upward shift of in the three maps is caused by the thermal drift of the stage during the measurement.

the larger scattering volume due to the 40 nm high SiGe line structures, the enhanced Raman signature from the Si substrate is unexpected. Due to the higher absorption by the SiGe patterns above a lower substrate signal would have been expected. The intensity of both Si–Si modes increases slightly already in a distance of about 800 nm from the lines reaching a maximum around the center of the SiGe pattern. Therefore, the far-field signal enhancement is attributed mainly to scattering of light by the nano-scale surface structures. As expected, a resolution of the five SiGe lines by confocal far-field Raman measurements is not possible (Fig. 4).

The enhanced electric field around the laser-irradiated tip apex acts as a nano-scale light source and should provide under optimized conditions an improved spatial resolution when scanning the sample surface with the metalized tip. The scans are performed in semi-contact mode enabling to keep a small average tip–sample distance of a few nm while measuring the surface modulated intensity variations of the Si–Si mode from SiGe and Si substrate. In Fig. 5 the AFM data obtained from a line scan and the Raman intensities of the two Si–Si modes in the spectral interval from 507 cm^{-1} to 512 cm^{-1} and 519 cm^{-1} to 522 cm^{-1} are shown. The corresponding AFM image and the two TER intensity maps are presented on the right beside the cross section data. From the AFM cross section data the distance between the neighboring lines is determined, showing for the scan a line spacing between 80 nm and 125 nm. In the corresponding AFM image (right side) the five about 40 nm high lines appear as bright stripes. The acquired Raman signal of the Si–Si mode from the Si substrate shows the same intensity increase around the structures as also observed in the scan performed with a retracted tip. However, in contrast to the far-field scan the intensity of the substrate signal decreases slightly at the position of each SiGe line due to the increase of the layer thickness from about 10 nm to 50 nm. The strong electromagnetic field around the tip enhances the Raman signal in a distance of about 30 nm around the tip apex [35]. Due to this strong decay of the near-field, the TER contribution to the Si substrate signal vanishes below the SiGe lines, thus leaving only the far-field contribution to the detected Raman intensity. In the corresponding TER intensity map the five lines appear therefore as dark stripes. For the SiGe signal exactly the opposite behavior was observed. The detected signal increases at the position of each SiGe line due to the larger scattering volume and decreases again between the lines where the layer thickness drops below 10 nm. The bright stripes in the corresponding TER intensity map indicate the position of the five SiGe lines. Due to the high surface sensitivity of the TER technique and the less intensive SiGe background signal the line structures are more clearly visible in the SiGe intensity map than in the according Si intensity map.

In Fig. 6 two TER spectra obtained from a line scan are compared. One spectrum (black) is acquired in a distance of about 500 nm from the pattern while the second spectrum (red) is taken from a SiGe line. The fit of both spectra with two Lorentz functions enables the determination of the band position, yielding for the Si–Si mode peaks $\omega=520.6\text{ cm}^{-1}$ (Si) and $\omega=513.1\text{ cm}^{-1}$ (SiGe) for the reference spectrum beneath the structures and $\omega=520.5\text{ cm}^{-1}$ (Si) and $\omega=509.9\text{ cm}^{-1}$ for the spectrum obtained from the SiGe line. The changed peak positions indicate a different stress state within the remnant SiGe layer and the free-standing SiGe line.

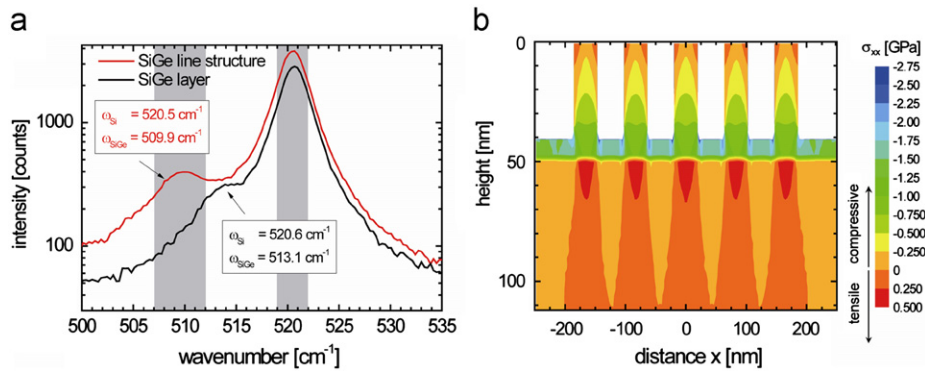


Fig. 6. (a) SiGe TER spectra obtained from a SiGe line (red) and an area several μm away from the surface structures (black). The peak position from the Si–Si mode from SiGe layer and Si substrate were obtained by fitting of the spectra with two Lorentz functions. (b) Stress distribution of the σ_{xx} component within the SiGe lines and the substrate below obtained by FEM calculations. The stress relaxation within the lines from the initial stress value (-1.53 GPa) leads to a redistribution in the remnant 10 nm thick SiGe layer and the Si substrate. (For interpretation of the references to color in this figure legend, the reader is referred to the web version of this article.)

In order to determine the reason for the observed peak shifts the stress distribution for a comparable pattern is calculated by finite element modeling (Fig. 6b). The obtained results show that the intrinsic stress within the remnant 10 nm thick SiGe layer is not affected by the patterning process ($\sigma_{xx}=\sigma_{yy}=\sigma_0=-1.53$ GPa). However, for the five free-standing SiGe lines and the substrate underneath a strong stress redistribution is observed. Due to the length of about 15 μm the stress component σ_{yy} parallel to the lines is not affected by stress relaxation. However, for the stress component σ_{xx} perpendicular to the SiGe lines a strong relaxation occurs (Fig. 6b). This relaxation of the compressive stress leads to the spectral shift of the Si–Si mode peak from its fully strained initial position at 513.1 cm^{-1} to 509.9 cm^{-1} . For the calculation of the stress component σ_{xx} within the SiGe lines from the experimentally obtained data the empirically derived relation from reference [36] and the stress model proposed by Jain et al. [37] are used. For this model it is assumed that the stress component σ_{yy} along the lines remains unchanged and corresponds to the initial stress value ($\sigma_{yy}=\sigma_0=-1.53$ GPa). The stress component perpendicular to the lines σ_{xx} can be described by the following equation:

$$\frac{\sigma_{xx}}{\sigma_0} = 1 - \frac{2}{\beta_1 \chi_{\text{Ge}}} (\omega_{\text{SiGe}} - \omega_{\text{Si,ref}} - \alpha_1 \chi_{\text{Ge}})$$

$\alpha_1 = -62 \text{ cm}^{-1}$ and $\beta_1 = 30.5 \text{ cm}^{-1}$ are material parameters [36] and χ_{Ge} denotes the Ge-concentration within the SiGe layer. $\omega_{\text{Si,ref}}$ represents the position of the stress-free Si reference position which is determined from the unpatterned area of the sample with a retracted TER tip in order to avoid a contribution from of the tip material to the measured Raman signal. **From the spectra acquired from the TER measurements a stress value of about $\sigma_{xx} = -190$ MPa is calculated, corresponding to a stress relaxation of about 88% compared to the initial value before patterning. The relaxation of the compressive stress within the SiGe lines induces also tensile stress in the substrate below the lines as shown in Fig. 6b. This small amount of the tensile stress could be the reason for the observed slight spectral shift of the Si substrate peak to lower wavenumbers (see Fig. 6 a) compared to the stress-free peak position. However, one has to consider, that the acquired spectral information describes only the right tendency for the Si substrate.** For a reliable characterization of the stress distribution within the Si substrate from the experimental data, the contribution of the tip material has to be eliminated completely.

4. Conclusions

In summary, we could show that by taking into account the orientation of the bulk crystalline samples the intensive

background signal in near-field Raman investigations can be reduced considerably while keeping the favorable laser polarization along the TER tip axis at the same time. The described configuration enables the acquisition of high-resolution TER images from SiGe structures with a line width between 20 and 40 nm despite the chemical identity of the sample surface. From the acquired spectra the intrinsic stress within the free-standing SiGe line structures can be determined. The achieved results demonstrate the capability of this technique to characterize the stress in Si based nanostructures with a spatial resolution required for the investigation of present leading edge CMOS devices. With further progress in preparation of metalized AFM-tips, TER spectroscopy could become a similar important non-destructive metrology technique for semiconductor industry as confocal Raman spectroscopy before.

Acknowledgment

The TER system was kindly provided by the NT-MDT company. Helpful discussions and support by Phillip Olk, Thomas Härtling, Andreas Hille and co-workers from IAPP are gratefully acknowledged by the authors. We also thank Ina Ostermay and Andreas Naumann from Fraunhofer CNT for providing the SiGe samples and David Lehninger and Sven Niese from Global Foundries Dresden for support during the measurements.

References

- [1] Y. Sun, S.E. Thompson, T. Nishida, *Journal of Applied Physics* 101 (2007) 104503.
- [2] M.L. Lee, E.A. Fitzgerald, M.T. Bulsara, M.T. Currie, A. Lochtefeld, *Journal of Applied Physics* 97 (2005) 011101.
- [3] T. Kammiller, I. Pedėjus, A. Wei, K. Romero, C. Reichel, S. Heinemann, H.-J. Engelmann, *ESC Transactions* 3 (7) (2006) 713–718.
- [4] M. Bauer, D. Weeks, Y. Zhang, V. Machkaostan, *ESC Transactions* 3 (7) (2006) 187–196.
- [5] S. Flachowsky, R. Illgen, T. Herrmann, W. Klíx, R. Stenzel, I. Ostermay, A. Naumann, A. Wei, J. Hontschel, M. Horstmann, *Journal of Vacuum Science and Technology B* 28 (2010) C1G12.
- [6] M.V. Fischetti, S.E. Laux, *Journal of Applied Physics* 80 (1996) 2234.
- [7] M.L. Lee, E.A. Fitzgerald, M.T. Bulsara, M.T. Currie, A. Lochtefeld, *Journal of Applied Physics* 97 (2005) 011101.
- [8] R. Loudon, *Advances in Physics* 13 (52) (1964) 423–482.
- [9] I. de Wolf, H.E. Maes, S.K. Jones, *Journal of Applied Physics* 79 (1996) 9.
- [10] V. Poborchii, T. Tada, T. Kanayama, *Applied Physics Letters* 91 (2007) 241902.
- [11] P.H. Tan, D. Bougeard, G. Abstreiter, K. Brunner, *Journal of Applied Physics* 98 (2005) 113517.
- [12] P. Hermann, M. Hecker, F. Renn, M. Rölke, K. Kolanek, J. Rinderknecht, L.M. Eng, *Journal of Applied Physics* 109 (2011) 124513.
- [13] K. Kneipp, M. Moskovits, H. Kneipp, *Surface-Enhanced Raman Scattering: Physics and Applications*, Topics in Applied Physics, vol. 103, Springer Verlag, Berlin, 2006.

- [14] R.M. Stöckle, Y.D. Suh, V. Deckert, R. Zenobi, *Chemical Physics Letters* 318 (2000) 131.
- [15] B. Pettinger, *Tip-enhanced Raman Spectroscopy (TERS)*, Topics in Applied Physics, vol. 103, Springer Verlag, Berlin, 2006, pp. 217–240.
- [16] W.X. Sun, Z.X. Shen, *Ultramicroscopy* 94 (2003) 237–244.
- [17] L. Zhu, C. Georgi, M. Hecker, J. Rinderknecht, A. Mai, Y. Ritz, E. Zschech, *Journal of Applied Physics* 101 (2007) 104305.
- [18] N. Hayazawa, M. Motohashi, Y. Saito, H. Ishitobi, A. Ono, T. Ichimura, P. Verma, S. Kawata, *Journal of Raman Spectroscopy* 38 (2007) 684–696.
- [19] N. Lee, R.D. Hartschuh, D. Mehtani, A. Kisliuk, J.F. Maguire, M. Green, M.D. Foster, A.P. Sokolov, *Journal of Raman Spectroscopy* 38 (2007) 789–796.
- [20] M. Motohashi, N. Hayazawa, A. Tarun, S. Kawata, *Journal of Applied Physics* 103 (2008) 034309.
- [21] N. Anderson, A. Bouhelier, L. Novotny, *Journal of Optics A: Pure and Applied Optics* 8 (2006) 227–233.
- [22] L.G. Cancado, A. Hartschuh, L. Novotny, *Journal of Raman Spectroscopy* 40 (2009) 1420.
- [23] J. Steidtner, B. Pettinger, *Physical Review Letters* 100 (2008) 236101.
- [24] P. Olk, J. Renger, T. Härtling, M.T. Wenzel, L.M. Eng, *Nano Letters* 7 (6) (2007) 1736–1740.
- [25] P.M. Campbell, E.S. Snow, P.J. McMarr, *Applied Physics Letters* 66 (11) (1995).
- [26] K. Kolanek, P. Hermann, P.T. Dudek, T. Gotszalk, D. Chumakov, M. Weisheit, M. Hecker, E. Zschech, *Thin Solid Films* 12 (518) (2010) 3267–3272.
- [27] A. Hartschuh, *Angewandte Chemie International Edition* 47 (2008) 8178–8191.
- [28] A. Tarun, N. Hayazawa, S. Kawata, *Analytical and Bioanalytical Chemistry* 394 (2009) 1775–1785.
- [29] A. Bouhelier, *Microscopy Research and Technique* 69 (2006) 563–579.
- [30] L. Novotny, B. Hecht, *Principles of Nano-Optics*, Cambridge University Press, New York, 2006.
- [31] P.G. Gucciardi, M. Lopes, R. Déturche, C. Julien, D. Barchiesi, M. Lamy de la Chapelle, *Nanotechnology* 19 (2008) 215702.
- [32] R. Schorer, G. Abstreiter, S. de Gironcoli, E. Molinari, H. Kibbel, H. Presting, *Physical Review B* 49 (8) (1994) 5406–5414.
- [33] I. De Wolf, H. Norström, H.E. Maes, *Journal of Applied Physics* 74 (1993) 7.
- [34] K.F. Domke, B. Pettinger, *Journal of Raman Spectroscopy* 40 (2009) 1427–1433.
- [35] B. Pettinger, K.F. Domke, D. Zhang, G. Piccardi, R. Schuster, *Surface Science* 603 (2009) 1335–1341.
- [36] M. Hecker, L. Zhu, C. Georgi, I. Zienert, J. Rinderknecht, et al., *AIP Proceedings* 931 (2007) 435.
- [37] S.C. Jain, B. Dietrich, H. Richter, A. Atkinson, A.H. Harker, *Physical Review B* 52 (1995) 9.